Engineering and Applied Science Letters

PSR Press

Article

Lightning as an effective topological transition in the electromagnetic Gauge field

Mykola Yaremenko

The National Technical University of Ukraine, Kyiv, Ukraine; math.kiev@gmail.com.

Received: 23 April 2026; Accepted: 19 June 2026; Published: 22 June 2026.

Abstract: In this paper, we develop an effective gauge-theoretic description of atmospheric electrical breakdown where the transition from weakly conducting air to a lightning channel is described via an order parameter instability. The formulation includes the interaction of the degree of ionization and the collective conducting amplitude with the electromagnetic potential. The key question is whether regularities found in lightning initiation, stepped leader propagation, channel confinement, and branching can be captured using topological invariants or just via threshold values of fields. Our model defines the critical field strength to be the point where the conducting order parameter becomes unstable, derives vortex channel solutions with a finite core and an effective flux increment, and connects branch geometry to symmetrically constrained weight vectors. We also describe the limited role played by instanton-like nucleation, anomalous transport terms, and dual confinement within the framework of an effective description rather than as a microscopically justified one. Predictions derived within our approach are formulated in terms of measurable quantities: vortex core length scales, branch angle clustering, field-temperature scaling, radio signals polarization dependence, and magnetic field increment near developing channels.

Keywords: lightning discharge, atmospheric electricity, gauge theory, topological defects, dielectric breakdown, vortex solutions

1. Introduction

Atmospheric lightning is a strongly nonlinear discharge process characterized by a variety of phenomena at different scales such as electric currents up to 10^5 A, channel heating, high energy emission, and streamer–leader dynamics [1–3]. The standard descriptions focus on the initiation through field enhanced ionization, electron avalanches, streamers, and conductivity feedback. This framework is essential, yet not sufficient for the description of geometric lightning regularities such as channel confinement, stepping, branching, and scale dependence [4–6].

The objective of the current paper is the reformulation of those geometric properties in terms of effective fields and topology. It is crucial that the word *effective* is used in its literal meaning, as no new gauge particles or high energy vacuum state in the atmosphere is implied. On the contrary, this work relies on the mathematical construction of gauge theory to describe collective electrodynamic fields such as the electromagnetic potential, ionization or polarization, and conducting order parameter of the developing plasma. This approach is meaningful only if it predicts measurable effects that can be compared to high speed imaging, radio interferometry, magnetometry, and satellites data [7–9].

The key research question can be formulated as follows: Is it possible to describe the initiation and propagation of lightning in the framework of effective topological phase transition whose manifestations will be critical field of breakdown, vortex-like conducting channels, branching with symmetry constraints, and flux confinement? The innovation consists in bringing together four different quantities: order parameter instability, finite energy vortex, branching geometry, and measurement tools. This allows formulating a mathematically rigorous framework for the description of lightning morphology and keeping connection to physical processes.

The organization of the paper is as follows: the effective fields and critical point are defined in §2. The vortex-like channel and corresponding characteristic lengths are derived in §3. In §4, the branching problem is treated as the symmetry constrained network. In §5, the instanton-like nucleation is presented as a controlled

analogy for rare streamer seeds. In §6, the additional terms related to anomalous transport are included for the case of polarization-resolved emissions. In §7, the concept of flux confinement and Wilson loop measurement are introduced. The results are discussed in figures and tables in §8. The conclusion with discussion of contributions and limitations is given in §9.

2. Gauge-theoretic formulation of atmospheric breakdown

2.1. Effective fields and physical interpretation

Let $A_\mu = (\phi/c, \boldsymbol{A})$ be the electromagnetic potential and $F_{\mu\nu} = \partial_\mu A_\nu - \partial_\nu A_\mu$ the field tensor. Two collective variables are introduced. The real variable σ describes the bound-charge polarization or ionization resistance, where larger σ denotes the dielectric phase. The complex variable $\psi = fe^{i\theta}$ is the amplitude of the conducting phase of the plasma with $|\psi|^2$ measuring a coarse-grained density of electrons. The charge q in the covariant derivative

$$D_\mu \psi = (\partial_\mu - iqA_\mu)\psi, \tag{1}$$

is therefore an effective coupling that connects the collective conducting phase to the electromagnetic potential.

The local Lagrangian density is written as

$$\mathcal{L} = -\frac{1}{4}\epsilon(\sigma, |\psi|^2)F_{\mu\nu}F^{\mu\nu} + |D_\mu\psi|^2 + \frac{1}{2}\partial_\mu\sigma\partial^\mu\sigma - V(\psi, \sigma), \tag{2}$$

where

$$\epsilon(\sigma, |\psi|^2) = 1 + g_1\sigma + g_2\sigma^2 + g_3|\psi|^2, \tag{3}$$

allows a field-dependent dielectric response, and

$$V(\psi, \sigma) = \lambda_\psi(|\psi|^2 - v_\psi^2)^2 + \lambda_\sigma(\sigma^2 - v_\sigma^2)^2 + \kappa|\psi|^2\sigma^2. \tag{4}$$

This potential separates the dielectric state, in which $\langle\sigma\rangle$ is nonzero and $\langle\psi\rangle = 0$, from the conducting state, in which $\langle\psi\rangle$ becomes nonzero and the polarization barrier is reduced.

2.2. Critical field and order-parameter instability

For a background electric field with $B \ll E$, the conducting field has an effective mass

$$m_\psi^2(E) = m_0^2 - \alpha E^2, \qquad m_0^2 = \kappa v_\sigma^2 - \lambda_\psi v_\psi^2, \tag{5}$$

where $\alpha > 0$ collects the field-dependent part of the dielectric coupling. The critical field is therefore

$$E_c = \sqrt{\frac{m_0^2}{\alpha}}. \tag{6}$$

For the case when $E < E_c$, the perturbations in ψ vanish, and the air is essentially dielectric. However, when $E > E_c$, the conducting perturbation amplitude becomes larger, and the channel may develop. The critical electric field should not be regarded as a substitute for empirically determined breakdown electric fields, but only a stability condition for fitting.

The finite-temperature correction can be summarized by

$$E_c(T) = E_c(0)\left[1 - \left(\frac{T}{T_0}\right)^2\right]^{1/2}, \tag{7}$$

which is the transition curve depicted in Figure 1. It should be stressed that the theory gives rise to a whole family of thresholds, instead of a unique universal number. This issue is relevant to atmospheric applications since cloud microphysics affects local effective temperature, density, and ionization history.

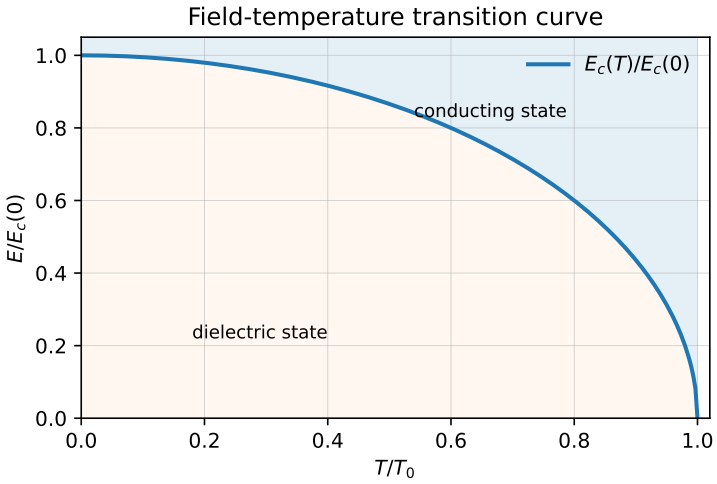

Figure 1. Effective field-temperature transition curve. The lower part of the diagram corresponds to the stable dielectric state, whereas the upper part corresponds to the growth of the conducting order parameter

Figure 1 does not mean that lightning is driven only by temperature. On the contrary, it shows how the critical field becomes a state-dependent quantity. An important application of the picture is a comparison of the derived threshold values with the initiation radio or optical observations. The presence of the systematic correlation of initiation with the curve of the type (7) proves the theory of topological transition. The absence of the scaling law falsifies the formulation.

3. Topological defects in atmospheric breakdown

3.1. Vortex ansatz for a conducting channel

Once the conducting amplitude gets nonzero, finite-energy vortex-type defects may describe narrow conducting channels. Assuming a straight channel oriented along the z axis, one can consider a cylindrical ansatz

$$\psi(r,\varphi) = f(r)e^{in\varphi}, \qquad A_\varphi(r) = \frac{n}{q}\frac{a(r)}{r}, \qquad \sigma(r) = s(r), \tag{8}$$

where $n \in \mathbb{Z}$ is the winding number. Regularity and finite energy require

$$f(0) = 0, \quad a(0) = 0, \quad s(0) = s_0, \qquad f(\infty) = v_\psi, \quad a(\infty) = 1, \quad s(\infty) = 0. \tag{9}$$

The magnetic field along the core is

$$B_z(r) = \frac{1}{r}\frac{\mathrm{d}}{\mathrm{d}r}\left[rA_\varphi(r)\right] = \frac{n}{q}\frac{a'(r)}{r}. \tag{10}$$

The flux through the channel core is

$$\Phi = \int B_z \,\mathrm{d}S = \oint A_\varphi r \,\mathrm{d}\varphi = \frac{2\pi n}{q}. \tag{11}$$

Eq. (11) must be understood as an effective increment in the flux. Its value is based on the estimated coupling coefficient q rather than on the actual superconducting value $2e$. This remark solves the problem of ambiguity concerning the quantization hypothesis and makes the statement testable: magnetic-field circulation around emerging leaders should be concentrated around multiples of the increment if the hypothesis about vortices is correct.

3.2. Core sizes and magnetic fields

Linearization in the conducting phase provides three characteristic lengths:

$$\xi_\psi = m_\psi^{-1}, \qquad \lambda_A = m_A^{-1}, \qquad \xi_\sigma = m_\sigma^{-1}. \tag{12}$$

Here ξ_ψ is the coherence length for the conducting amplitude, λ_A is the electromagnetic penetration depth, and ξ_σ is the recovery length of the polarization field. One can observe the typical structure of the fields in Figure 2: the conducting amplitude is suppressed at the center and then recovered, the gauge field screens the magnetic field, and the polarization variable has maximum values in the transition zone.

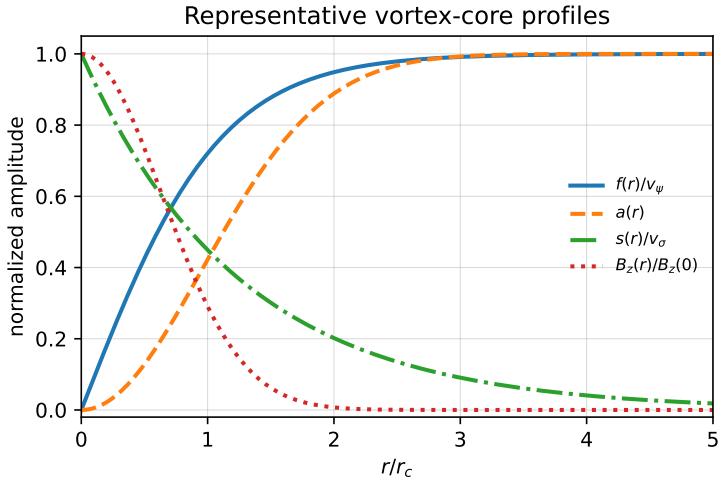

Figure 2. Representative vortex-channel profiles normalized by their asymptotic or central values. The curves show how the conducting amplitude, gauge profile, polarization field, and axial magnetic field occupy different radial scales

The physical meaning of the vortex presented in Figure 2 is that the lightning channel is not an extremely sharp geometric object within this model. It consists of several layers, namely, the ionized core, the electromagnetic shielding layer, and the layer of polarization recovery. Hence, the estimates of the optical width of the channel will give us an incomplete picture of the actual size of the electromagnetic vortex.

Table 1 contains a division of the mathematical parameters into measurable observables. This is needed, since the topological model becomes scientifically meaningful only if we are able to measure or falsify some of its parameters. In addition, Table 1 corrects one of the frequent overinterpretations – the winding number is not observable by taking a photograph of the branch but should be deduced from circulation, core structure, or measurements of channels' family.

Table 1. Effective parameters and observational roles

Parameter	Model role	Observable interpretation
E_c	Onset of conducting-amplitude instability	Local initiation threshold after correction for density, humidity, and hydrometeor state
ξ_ψ	Conducting-core length scale	Optical or plasma-density channel radius
λ_A	Electromagnetic penetration scale	Magnetic and radio-field width around the channel
ξ_σ	Polarization-recovery scale	Region over which surrounding air remains field-conditioned
n	Winding number of the channel	Integer ordering of magnetic circulation if present
q	Effective gauge coupling	Fitted scale that converts circulation into the flux increment

4. Non-abelian branching description

4.1. Branching as a constrained network

Non-abelian gauge fields may be able to describe branch angles if discharge channels are viewed as directions in the internal weight space. This analysis presents it as a hypothesis on the symmetry-constrained network of channels. If we have the local conducting order parameter with N components Φ_i, transforming under $\mathrm{SU}(N)$, then the minimal field tensor is

$$F^a_{\mu\nu} = \partial_\mu A^a_\nu - \partial_\nu A^a_\mu + g f^{abc} A^b_\mu A^c_\nu, \tag{13}$$

and the covariant derivative is

$$D_\mu \Phi_i = \partial_\mu \Phi_i - \mathrm{i} g A^a_\mu (T^a)_{ij} \Phi_j. \tag{14}$$

A branch junction is then represented by a local conservation rule in weight space,

$$w_1 + w_2 + w_3 = 0, \tag{15}$$

where the vectors w_i encode the preferred internal directions of the emerging channels.

In the case of the most simple triangular weight set, the outgoing directions are spaced by 120°, see Fig. 3. This figure makes more explicit a previously implicit verbal analogy. It does not assert that every branch must emerge at precisely 120°, but rather specifies the angular set one expects to arise from a junction point regulated by the triangular weight condition.

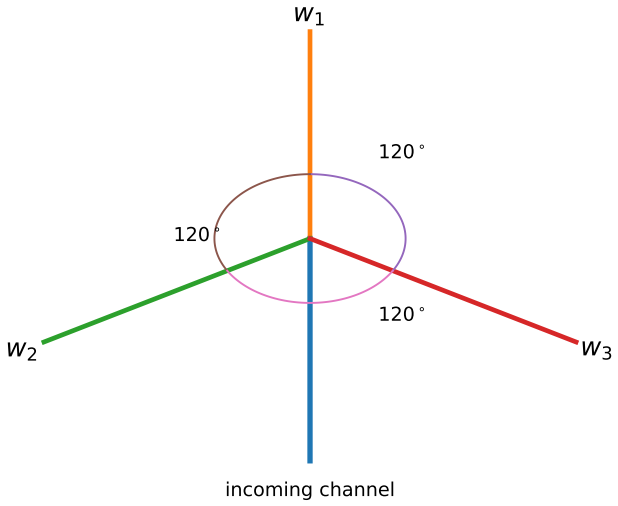

Figure 3. Symmetry-constrained branch junction with three weight vectors satisfying $w_1 + w_2 + w_3 = 0$. The triangular relation provides the preferred angular spacing of 120°

The relevance of Fig. 3 is interpretive, not decorative. A random fractal branching mechanism will produce any number of branch angles, but it does not itself specify a preferred cluster of angularities. The non-abelian approach suggests that the histogram of branch angles should stabilize into a clear peak once corrections for projection, age of the channel, and viewing geometry have been taken into account. This prediction needs to be verified by three dimensional rapid imaging techniques, not merely by two dimensional photographs.

4.2. Branch statistics and current partition

Let $P(w,t)$ be the probability of occupying a local weight direction w on the growing tip. A simple stochastic equation is

$$\frac{\mathrm{d}P(w,t)}{\mathrm{d}t} = \sum_{w'} \left[W(w' \to w)P(w',t) - W(w \to w')P(w,t) \right], \tag{16}$$

where W is a transition rate on the weight lattice. The branching process will occur when the energy released through electromagnetic radiation is larger than the cost of creating two channel cores. The current ratio can be calculated by using the junction coefficient,

$$\frac{I_{\text{branch}}}{I_{\text{main}}} = \left| \frac{C^{w_3}_{w_1 w_2}}{C^{w_2}_{w_1 w_1}} \right|^2. \tag{17}$$

The findings presented in Table 2 transform the branching argument into an experimental set of criteria. Rather than requiring the presence of a 120° angle from a single photograph, the critical criterion will be the presence of an angular excess with associated current ratios after correction. If the angular distribution becomes continuous upon reconstruction in three dimensions, the non-abelian model is ruled out.

Table 2. Branching diagnostics implied by the symmetry-constrained description

Diagnostic	Expected pattern	Interpretation
Branch angle	Persistent cluster near triangular separation	Evidence for weight-space selection rather than purely random growth
Current partition	Repeatable ratio between main and secondary channels	Junction coefficient has measurable electrodynamic content
Branch hierarchy	Approximate scale similarity over a limited range	Network growth repeats local symmetry constraints
Projection sensitivity	Strong change between 2D and 3D angle statistics	Apparent peaks may be imaging artifacts if not corrected

5. Streamer seed generation through instanton-type nucleation

Streamer generation happens under a metastable field condition whereby many of the avalanches do not succeed while only few of them succeed in forming leaders. Nucleation via a non-perturbative process is thus important, although it should not be interpreted literally as quantum mechanical tunneling at macroscopic scales. The action for a non-abelian field in Euclidean coordinates is

$$S_E = \frac{1}{4g^2} \int F^a_{\mu\nu} F^a_{\mu\nu} \, \mathrm{d}^4 x, \tag{18}$$

with topological charge

$$Q = \frac{g^2}{32\pi^2} \int F^a_{\mu\nu} \widetilde{F}^a_{\mu\nu} \, \mathrm{d}^4 x, \qquad \widetilde{F}^a_{\mu\nu} = \frac{1}{2} \epsilon_{\mu\nu\rho\sigma} F^a_{\rho\sigma}. \tag{19}$$

The nucleation rate is represented by

$$\Gamma(E) \simeq \Gamma_0 \exp\left[-S_0 \left(1 - \frac{E^2}{E_c^2} \right)^2 \right], \tag{20}$$

where S_0 is the effective action associated with an activation. The Eq. (20) exhibits the right behavior: nucleation is suppressed far from the threshold and sharply increases when the field is close to E_c.

Streamer development can then be treated as a two-particle interaction problem for a nucleation seed and its growing counterpart. The potential energy for such interaction, if R is the separation distance, has the form

$$V(R) = -\frac{12\pi^2}{g^2} \frac{\rho^2 \rho'^2}{R^4} + O(R^{-6}), \tag{21}$$

where ρ and ρ' are effective seed sizes. In essence, it should be viewed as an approximation scheme for a rare process of initiation. The observable manifestation of the effect will be a very nonlinear increase in the initiation rate with approaching the critical field.

That restricts our claim. One does not need instanton language to describe each electron avalanche; it is needed only for the rare ones which live long enough to be optically and electromagnetically detected as streamers. This makes the distinction clear since before one tended to confuse microscopic ionization with macroscopic streamer propagation.

6. Chiral and anomalous transport terms

The rapid change of electric and magnetic fields in a discharge produces the polarization-dependent electromagnetic signal. For description of these effects the effective action might include the pseudoscalar term

$$\mathcal{L}_\theta = \frac{\theta_{\text{eff}}}{32\pi^2} F_{\mu\nu}\widetilde{F}^{\mu\nu}, \tag{22}$$

where θ_{eff} is an atmospheric effective coefficient rather than a fundamental vacuum angle. The associated anomalous current can be written as

$$\boldsymbol{J}_{\text{anom}} = \gamma_5 \mu_5 \boldsymbol{B} + \gamma_E \nabla\theta_{\text{eff}} \times \boldsymbol{E}, \tag{23}$$

where μ_5 represents local asymmetry in handedness and γ_5, γ_E are fitted parameters for transport.

The meaning of Eq. (23) is important because it suggests that some emissions will not only depend on the magnitude of the field, but also on polarization, helicity, and the sign of $\boldsymbol{E}\cdot\boldsymbol{B}$. This suggestion may be checked by wideband radio interferometry and satellites which carry polarization data. In case the polarized data reveals no $\boldsymbol{E}\cdot\boldsymbol{B}$ correlation after subtraction of all known contributions to plasma effects, the anomalous transport contribution of the theory must be rejected.

7. Dual Confinement and Channel Stability

The lightning channel is confined to a small cross section in spite of releasing a large amount of energy per discharge. Dual Confinement explains such behavior through the string tension, which is the cost for the spread of the electric flux. The Wilson loop

$$W(C) = \left\langle \exp\left(\mathrm{i}q \oint_C A_\mu \, \mathrm{d}x^\mu \right) \right\rangle, \tag{24}$$

serves as an order parameter for the effective medium. In the dielectric state, the loop is expected to follow a perimeter-type behavior,

$$-\ln W(C) \propto P(C), \tag{25}$$

where $P(C)$ is the contour perimeter. In the conducting channel state, confinement of field lines gives an area contribution,

$$-\ln W(C) = \sigma A(C) + \eta P(C) + \cdots, \tag{26}$$

with string tension

$$\sigma(E) = \sigma_0 \left(\frac{E - E_{\text{c}}}{E_{\text{c}}} \right)^{\nu}, \qquad E > E_{\text{c}}. \tag{27}$$

Here ν is an important exponent that can be related to universality classes described by phase-transition theory [10–12].

The area-law relation is meaningful because it relates channel stability to a physical variable. The higher σ, the greater confinement and weaker expansion. Vanishing σ means unstable initiation, diffuse streamers, or channel failure. In other words, the area law allows one to relate the appearance of conductivity, existence of a stable leader core, and the shift in channel behavior from diffuse corona activity into a narrow conductor.

8. Results and discussion

8.1. Analytical predictions

The major prediction is the emergence of the same effective variables that control four discharge properties: breakdown threshold, channel core, branch junction, and EM confinement. Critical field condition (6) determines the onset of conducting-amplitude instability. Vortex ansatz (8) leads to a finite channel core with a measurable flux change (11). Branching condition (15) determines the preferred junction geometry. Wilson loop form (26) relates channel stability to the quantity similar to string tension. These relations are related and cannot be considered separately; the model describing one but not the other will be inconsistent.

Consequences are clear: the evaluation of lightning morphology should not rely on one diagnostic variable only. Optical measurements can provide the geometry of branches but cannot check the increment of flux. Magneto-optical measurements can determine the current circulation but cannot by themselves distinguish between projection and real angles. Radio interferometry can provide information about the three-dimensional geometry and polarization but still requires local electric field measurement. Table 3 summarizes the minimum diagnostics required.

Table 3. Predicted signatures and required measurements

Model component	Predicted signature	Measurement requirement
Critical transition	State-dependent threshold $E_c(T)$	Local field reconstruction with environmental correction
Vortex channel	Finite core and effective flux increment	Magnetic-field circulation and optical/radio channel width
Branch network	Excess of triangular branch separations	Three-dimensional branch-angle statistics
Nucleation term	Rapid rise of initiation probability near E_c	Synchronized field, optical, and radio onset data
Anomalous transport	Polarization term correlated with $\boldsymbol{E} \cdot \boldsymbol{B}$	Full-Stokes radio or satellite measurements
Dual confinement	Area-law contribution and nonzero string tension	Lattice-style reconstruction from field maps or controlled laboratory discharge arrays

Table 3 also makes clear where the model fails. The prediction of branch angle depends on three-dimensional statistics being continuous after removing perspective effects. The prediction of flux depends on magnetic circulation being distributed smoothly between events instead of being clustered. The chiral term depends on polarization statistics not being entirely explained by ordinary plasma emission. These deficiencies make the paper stronger by providing an empirical edge instead of treating the theory as self-validating.

8.2. Explanation of the figures

The phase diagram in Figure 1 endows the critical field with a state-dependent character. What is important about the analytic function shown is not its accuracy in predicting exact thresholds but its general prediction that thresholds will collapse into a universal normalized curve upon corrections for environment. In Figure 2, the vortex profile shows that different measurements may report different channel radii, since optical emission, conducting current, and magnetic screening do not occur at identical radial distances. This explains why optical channel width does not necessarily equal radio and magnetic influence width.

Figure 3 helps to clarify the morphological prediction that a triangle will lead to a 120° branching angle. This figure is deliberately schematic since the assertion refers to angle statistics after correction and not to visual agreement with some particular lightning photograph. The diagnostic chart in Figure 4 correlates each prediction with its associated measurement technique.

The best immediate tests according to Figure 4 are magnetic arrays for flux increments, high speed optics for core and branch geometry, and radio mapping for polarization-sensitive diagnostics. Satellite magnetic field data are less useful for individual core structure but very useful for global distribution and $\boldsymbol{E} \cdot \boldsymbol{B}$ statistics. The figure therefore supports a multi-instrument strategy rather than a single observational test.

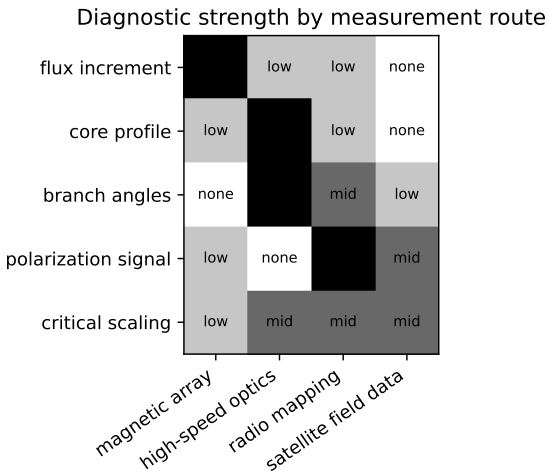

Figure 4. Diagnostic strength of proposed measurement routes for the main predicted signatures. The map distinguishes direct tests from supporting measurements

8.3. Implications and limitations of the formulation

The formulation brings a concise mathematical link between phase transition terminology and the morphological language of atmospheric discharge. The greatest success of the formulation lies in its vortex-channel module due to the linkage of instability of the field, finiteness of core and circulation. The branch network is more speculative but experimentally testable. Anomalous transport and dual confinement should be seen as modules only to be included in case when polarization and confinement patterns will not find explanation in terms of plasma physics.

There are three major limitations of the formulation. First, it is a coarse-grained approximation that cannot serve as a substitute for kinetic modeling and measurements of gas chemistry. Second, all its parameters are effective and should be obtained from atmospheric conditions rather than imported from elementary particle physics. Third, topological nature of the process demands an ensemble of data. Single photo and even single discharge cannot prove existence of winding, weight-space selection and confinement of the process.

9. Conclusions

The aim of this paper was to find out if lightning initiation, propagation, branching and channel confinement can be explained as an effective topological transition in the electromagnetic field. This paper provided the answer to this question on conditional basis by showing that coupled order-parameter description of the dielectric-to-conducting transition by means of instability of ψ is possible; vortex ansatz allows to produce a finite conducting channel with effective flux increment; triangular weight space relation predicts a clear branch angle; and Wilson loop description links channel stability and confinement.

The main contribution of this formulation does not lie in the replacement of standard lightning physics. It is in providing a mathematically consistent description of the aspects of lightning that would correspond to topological effects and observations that could falsify this statement. Predicted major signatures of topological transition in lightning are state-dependent critical scaling, vortex-core layered structure, magnetic circulation clustering, branch angle excess close to triangular separation, polarization sensitive radio interference terms and channel stability confinement pattern.

The conclusion is that the experimental testing of this idea should incorporate fast optical reconstruction, broadband radio interferometer, magnetic sensors and environmental field estimation. Success in such endeavor will bring a new vocabulary to discuss atmosphere electricity and phase transitions. Even if predicted signatures will not appear, this will define the boundaries of topological analogy and conventional discharge physics.

Conflicts of Interest: The author declares no conflict of interest.

References

[1] Iudin, D. I., Davydenko, S. S., Gotlib, V. M., Dolgonosov, M. S., & Zelenyi, L. M. (2018). Physics of lightning: new model approaches and prospects for satellite observations. *Physics–Uspekhi, 61*(8), 766-778.

[2] Marshak, I. S. (1962). Strong-current pulse (spark) discharges in gas, used in pulsed light sources. *Soviet Physics Uspekhi, 5*(3), 478-514.

[3] Jánský, J., Bessiéres, D., Brandenburg, R., Paillol, J., & Hoder, T. (2021). Electric field development in positive and negative streamers on dielectric surface. *Plasma Sources Science and Technology, 30*(10), 105008.

[4] Niemeyer, L., Pietronero, L., & Wiesmann, H. J. (1984). Fractal dimension of dielectric breakdown. *Physical Review Letters, 52*(12), 1033.

[5] Miranda, F. J., & Sharma, S. R. (2016). Multifractal analysis of lightning channel for different categories of lightning. *Journal of Atmospheric and Solar-Terrestrial Physics, 145*, 34-44.

[6] Goldberg, D. J., Nag, A., Cummins, K. L., Plaisir, M. N., Tempert, A., Brower, A. T., ... & Rassoul, H. K. (2026). Multi-frequency signatures of space-leader evolution in negative cloud-to-ground lightning stepped leaders. *Atmospheric Research, 2026*, 108835.

[7] Yin, W., Jin, W., Zhou, C., Liu, Y., Tang, Q., Liu, M., ... & Zhao, Z. (2021). Lightning detection and imaging based on VHF radar interferometry. *Remote Sensing, 13*(11), 2065.

[8] Shi, M., Zhang, W., Fan, P., Chen, Q., Liu, Z., Li, Q., & Liu, X. (2022). Modelling deep convective activity using lightning clusters and machine learning. *International Journal of Climatology, 42*(2), 952-973.

[9] Surkov, V. V., & Hayakawa, M. (2020). Progress in the study of transient luminous and atmospheric events: A review. *Surveys in Geophysics, 41*(5), 1101-1142.

[10] Kibble, T. W. (1976). Topology of cosmic domains and strings. *Journal of Physics A: Mathematical and General, 9*(8), 1387-1398.

[11] Donaire, M. (2006). Topological defects from first-order gauge theory phase transitions. *Journal of Physics A: Mathematical and General, 39*(48), 15013-15056.

[12] Fujimori, T., Iida, H., & Nitta, M. (2016). Field theoretical model of multilayered Josephson junction and dynamics of Josephson vortices. *Physical Review B, 94*(10), 104504.

[13] Nielsen, H. B., & Olesen, P. (1973). Vortex-line models for dual strings. *Nuclear Physics B, 61*, 45-61.

[14] Belavin, A. A., Polyakov, A. M., Schwartz, A. S., & Tyupkin, Y. S. (1975). Pseudoparticle solutions of the Yang-Mills equations. *Physics Letters B, 59*(1), 85-87.

[15] Coleman, S. (1985). *Aspects of Symmetry.* Cambridge University Press.

[16] Manton, N., & Sutcliffe, P. (2004). *Topological Solitons*. Cambridge University Press.

[17] Zel'Dovich, Y. B., & Raizer, Y. P. (2002). *Physics of Shock Waves and High-Temperature Hydrodynamic Phenomena.* Courier Corporation.